

To appear in The Astrophysical Journal

Detection of Far-Infrared Features in Star-Forming Regions¹

Takashi Onaka and Yoko Okada

*Department of Astronomy, Graduate School of Science, University of Tokyo, Bunkyo-ku,
Tokyo 113-0033, Japan*

onaka@astron.s.u-tokyo.ac.jp; okada@astron.s.u-tokyo.ac.jp

ABSTRACT

We report the detection of a feature at $65\mu\text{m}$ and a broad feature around $100\mu\text{m}$ in the far-infrared spectra of the diffuse emission from two active star-forming regions, the Carina nebula and Sharpless 171. The features are seen in the spectra over a wide area of the observed regions, indicating that the carriers are fairly ubiquitous species in the interstellar medium. A similar $65\mu\text{m}$ feature has been detected in evolved stars and attributed to diopside, a Ca-bearing crystalline silicate. The present observations indicate the first detection of a crystalline silicate in the interstellar medium if this identification holds true also for the interstellar feature. A similar broad feature around $90\mu\text{m}$ reported in the spectra of evolved stars has been attributed to calcite, a Ca-bearing carbonate mineral. The interstellar feature seems to be shifted to longer wavelengths and have a broader width although the precise estimate of the feature profile is difficult. As a carrier for the interstellar $100\mu\text{m}$ feature, we investigate the possibility that the feature originates from carbon onions, grains consisting of curved graphitic shells. Because of the curved graphitic sheet structure, the optical properties in the direction parallel to the graphitic plane interacts with those in the vertical direction in carbon onion grains. This effect enhances the interband transition feature in the direction parallel to the graphitic plane in carbon onions, which is suppressed in graphite particles. Simple calculations suggest that carbon onion grains are a likely candidate for the observed $100\mu\text{m}$ feature carrier, but the appearance of the feature is sensitive to the assumed optical properties.

¹Based on observations with ISO, an ESA project with instruments funded by ESA members states (especially the PI countries France, Germany, the Netherlands, and the United Kingdom) and with the participation of ISAS and NASA.

Subject headings: infrared: ISM – ISM: lines and bands – dust, extinction – ISM: individual (Carina nebula, Sharpless 171)

1. Introduction

Infrared spectroscopy provides a crucial means in the identification of interstellar dust compositions. Recent infrared satellite observations by the *Infrared Telescope in Space* (*IRTS*; Murakami et al. 1996) and the *Infrared Space Observatory* (*ISO*; Kessler et al. 1996) have revealed several new dust features in the diffuse emission, indicating the presence of new dust components in the interstellar medium (Onaka et al. 1996; Mattila et al. 1996; Chan & Onaka 2000). Observations by *ISO* also clearly show the presence of crystalline silicates around young and evolved stars for the first time (Waters et al. 1996; Waelkens et al. 1996; Kemper et al. 2002; Molster, Waters, & Tielens 2002), while it is not yet certain whether crystalline silicates exist commonly in interstellar space.

In the present paper we report the observations of active star-forming regions, the Carina nebula and the Sharpless 171 (S171) region with the Long-Wavelength Spectrometer (LWS; Clegg et al. 1996) on board *ISO* and the detection of far-infrared features around $65\,\mu\text{m}$ and $100\,\mu\text{m}$ in the diffuse emission. The Carina nebula is one of the most active regions on the Galactic plane and known to contain a number of early-type stars (Walborn 1995; Feinstein 1995). The S171 region is a typical H II region and molecular cloud complex (Yang & Fukui 1992). Both regions are supposed to represent the characteristics of active regions in the Galaxy. Possible carriers of the two detected features are discussed and we investigate the possibility that carbon onion grains of curved graphitic shells are the carrier for the broad interstellar $100\,\mu\text{m}$ feature.

2. Observations and Results

The central $40' \times 20'$ portion of the Carina nebula was observed by two-dimensional raster scans with the LWS full grating scan mode and the far-infrared spectra for $43\text{--}197\,\mu\text{m}$ were obtained for 132 positions (for details of the observations, see Mizutani, Onaka, & Shibai 2002). A one-dimensional scan was made for 24 positions on a line from the heating source to the molecular cloud region in S171 with the same LWS observing mode (Okada et al. 2002). The observed area of the both objects includes ionized regions and molecular clouds and the spectra sample the diffuse emission from the interstellar matter rather than the emission from point-like sources. The Off-Line Processing data of version 10.1 (OLP

10.1) provided by the ISO Archival Data Center were used in the present study. The spectra were defringed, converted into the surface brightness, and the extended source correction was applied by the ISO Spectral Analysis Package (ISAP²) software. The beam size and the correction factors were taken from the latest LWS Handbook (Gry et al. 2002). There are gaps in the spectra between the detector channels, which can be ascribed to the uncertainties either in the responsivity, in the dark current, or in the spatial brightness distribution in the beam.

Figure 1 shows examples of the obtained original spectra of the two regions, while Figure 2 indicates their stitched spectra to correct the gaps. Both spectra were taken at the interface regions between the molecular cloud and ionized gas, where the far-infrared intensity is sufficiently large to investigate dust features. The stitched spectra are made by scaling each detector signal because the observed regions are bright enough that the uncertainty in the dark current should be less significant than those in the responsivity or in the spatial brightness distribution. As can be seen in Figure 1, the amount of the gaps is small ($< \pm 5\%$) except for the three longest channels ($> 120 \mu\text{m}$), where 10–20% scaling is necessary to correct the gaps. The presence of a relatively narrow band feature at $65 \mu\text{m}$ is seen even in the unstitched spectra, particularly in S171. In the spectrum of the Carina nebula, the appearance of this feature is slightly disturbed by the higher levels of the adjacent channel spectra (SW2 and SW4) relative to the level of the SW3 channel, but it can still be seen in the individual spectrum of the SW3 channel. A broad feature centered around $100 \mu\text{m}$ is also noticeable in the unstitched spectrum of S171. The slope of the continuum starts to become flatter around the boundary between the SW4 and SW5 channels, indicating a feature starting around $80 \mu\text{m}$. In the unstitched spectrum of the Carina nebula, the gap between the SW4 and SW5 channels makes the feature less obvious, but the change in the slope in the SW5 channel can still be seen. The stitched spectrum clearly indicates the presence of the feature. However there is no appreciable abrupt change in the slope at longer wavelengths and the longer wavelength end of the feature is difficult to estimate from these spectra. Neither spurious features have been reported nor the relative spectral response functions have the corresponding features in these spectral ranges (Gry et al. 2002). We will discuss possible underlying continua to confirm the presence of the feature and estimate the feature profile in next section. Similar features are seen at about a half of the observed positions both in the Carina and S171 regions. Since these features are seen in a wide area of the interstellar medium, the band carriers must be ubiquitous species in interstellar space.

²The ISO Spectral Analysis Package (ISAP) is a joint development by the LWS and SWS Instrument Teams and Data Centers. Contributing institutes are CESR, IAS, IPAC, MPE, RAL and SRON.

3. Discussion

3.1. Interstellar $65\text{ }\mu\text{m}$ feature

Kemper et al. (2002) reported the presence of $65\text{ }\mu\text{m}$ and $90\text{ }\mu\text{m}$ features in the spectra of evolved stars. Figure 3a shows a spectrum of NGC6302 taken from the ISO Archival Data Center for comparison (cf. Molster et al. 2001). The continuum emission indicates a much higher temperature than those in Figure 2 and the features are weakly seen on the steep continuum. To see the features more clearly, the flux is multiplied by the square of the wavelength ($\lambda^2 F_\lambda$) and plotted in Figure 3b. The interstellar $65\text{ }\mu\text{m}$ feature seems very similar to that detected in evolved stars. The peak of the $65\text{ }\mu\text{m}$ feature is located obviously longer than [O I] $63\text{ }\mu\text{m}$ line (Fig. 4; see also Fig. 6) and thus is not compatible with the crystalline ice band at $62\text{ }\mu\text{m}$ (Smith et al. 1994; Molinari et al. 1999; Cohen et al. 1999). Koike et al. (2000) have proposed a Ca-bearing crystalline silicate, diopside ($\text{CaMgSi}_2\text{O}_6$), as a possible carrier of the $65\text{ }\mu\text{m}$ feature in evolved stars. Cryogenic measurements of the optical properties of diopside support the identification (Chihara, Koike, & Tsuchiyama 2001). Figure 4 shows a comparison of the observed spectra with the laboratory data. The best fit continua described in next subsection are also plotted. The laboratory spectrum shows a narrower profile than those observed and other species, such as water ice and dolomite ($\text{CaMg}(\text{CO}_3)_2$), have been suggested to contribute also to the $65\text{ }\mu\text{m}$ band emission (Kemper et al. 2002). Diopside has a weak feature also at $44.5\text{ }\mu\text{m}$. The LWS detector in this spectral range (SW1) is less sensitive and known to have strong hysteresis. In the present spectra a band feature is seen around $45\text{ }\mu\text{m}$ both in the upward and downward scans of both spectra, suggesting the presence of the $45\text{ }\mu\text{m}$ feature. However large noises in this spectral range preclude the firm detection and further observations are needed to confirm the feature. Band features of other crystalline minerals, such as the $69\text{ }\mu\text{m}$ band of forsterite seen in NGC6302, are not seen in the present LWS spectra. Diopside also has strong features in $30\text{--}40\text{ }\mu\text{m}$. The Carina nebula was observed by Short-Wavelength Spectrometer (SWS; de Graauw et al. 1996) and the spectra of $2.3\text{--}45\text{ }\mu\text{m}$ have been obtained. However the SWS spectra were not taken at the same positions as the LWS spectrum and thus the direct examination is difficult. The SWS spectra are dominated by strong continuum and do not clearly show any solid bands except for the broad $22\text{ }\mu\text{m}$ feature (Chan & Onaka 2000).

If the identification of the interstellar $65\text{ }\mu\text{m}$ with diopside is correct, this is the first detection of a crystalline silicate in the diffuse interstellar medium. Efficient destruction of dust grains by interstellar shocks suggests that a large fraction of interstellar dust must be formed in interstellar space in addition to those supplied from stars (Jones, Tielens, & Hollenbach 1996). Diopside is a high-temperature condensate and may survive harsh conditions. Calcium is a less abundant element than magnesium or silicon, but it is highly

depleted in the gas phase of the interstellar medium (Savage & Sembach 1996). Therefore the presence of Ca-containing dust should not be surprising in interstellar space. Based on the measured band strength of diopside (Chihara, Koike, & Tsuchiyama 2001) and the observed strength relative to the continuum, we roughly estimate that 5–10% of solar abundance calcium in diopside grains is sufficient to account for the observed band emission if we take the commonly used mass absorption coefficient of $50 \text{ cm}^2 \text{g}^{-1}$ for the continuum emission at $100 \mu\text{m}$ (Hildebrand 1983). Demyk et al. (1999) have suggested that the crystallinity of the silicates is less than 1–2% in the interstellar medium based on the observations of protostars.

3.2. Interstellar $100 \mu\text{m}$ feature

Since the feature seen around $100 \mu\text{m}$ is quite broad and weak, we investigate several cases for the underlying continuum to examine the presence of the broad $100 \mu\text{m}$ feature in detail and to make a rough estimate of the $100 \mu\text{m}$ feature profile. In the estimate of the continuum we assume the baseline positions to be at $55\text{--}60 \mu\text{m}$, $70\text{--}80 \mu\text{m}$, and $140\text{--}190 \mu\text{m}$ or $120\text{--}190 \mu\text{m}$ (see below) and we try to fit the observed spectra in these ranges with the model continuum as much as possible. Because the shortest spectral range ($55\text{--}60 \mu\text{m}$) has higher noises, less weight is put on this range in the fitting. We first adopt the dust model with the power-law emissivity ($\epsilon \propto \lambda^\beta$, where β is a constant) for the continuum emission. We found that the single-temperature graybody model cannot fit the entire baseline positions satisfactorily. Particularly the model always gives a higher flux at long wavelengths than the observed spectra. This discrepancy cannot be solved by increasing β because then the model would provide unnecessarily large fluxes at shorter wavelengths. Introducing a second component with a low temperature improves the fit drastically. The model of $\beta = 2$ both for warm and cold grains gives reasonable fits, but still has slightly larger fluxes at longest wavelengths ($\lambda > 160 \mu\text{m}$) than the observed spectra. Increase of β from 2 to unrealistically large 3 for the cold grains does not improve the fit appreciably.

The power-law emissivity model has a spectral dependence of $F_\lambda \propto \lambda^{-(4+\beta)}$ in the Rayleigh-Jeans regime. The discrepancy in the fit at longest wavelengths comes from the fact that the observed spectra have a gradually changing power-law index. The brightness distribution within the LWS beam affects the global shape of the spectrum. As shown in Figure 1 the unstitched spectra have relatively large gaps in longer wavelengths ($> 120 \mu\text{m}$), suggesting an uncertainty associated with the slope in this spectral range. It also suggests a difficulty in defining the assumed baseline in the longer wavelengths. In the following we present two cases for the baseline; one with $140\text{--}190 \mu\text{m}$ (case A) and $120\text{--}190 \mu\text{m}$ (case B) to examine the effect of the assumed baseline and as a more realistic model we examine

the astronomical silicate and graphite grain model (Draine & Lee 1984). The silicate and graphite grains both have approximately a power-law emissivity of $\beta \simeq 2$ in the far-infrared and this model provides slightly better fits than the power-law emissivity model of $\beta = 2$. We present the results of the silicate-graphite model in the following.

We assume different single temperatures for each of the astronomical silicate and graphite grains and search for the best fit temperatures. The observed regions may contain various temperature components of various dust grains and thus these fits are a simple approximation for the underlying continuum. In Figure 2 the best fit results are plotted together with the observed spectra. The dotted lines indicate the results for the case A baseline, which fit the observed spectra reasonably well even in the longest wavelengths. They overlap mostly with the observed spectra for $\lambda > 150 \mu\text{m}$ in the plot. The dashed lines show those for the case B baseline, which have obviously higher fluxes at longest wavelengths ($\lambda > 160 \mu\text{m}$) than the observed spectra. Both cases clearly indicate the presence of an excess feature starting around $80 \mu\text{m}$. The slope change around $80 \mu\text{m}$ is steep and cannot be accounted for by extra graybodies. The similarity of the excess profile in two different regions supports the presence of the feature and suggests the common origin.

Kemper et al. (2002) have attributed the $90 \mu\text{m}$ feature in evolved stars to calcite (CaCO_3), a carbonate mineral. In Figure 3b we also plot a single-temperature graybody as a simple reference continuum. Comparison with Figure 2 indicates that the $90 \mu\text{m}$ feature in NGC6302 is narrower than the interstellar $100 \mu\text{m}$ feature. The spectrum of NGC6302 shows a clear slope change around $100 \mu\text{m}$, which indicates the longer wavelength edge of the feature. In contrast, the interstellar spectra do not show the clear change in the slope and suggest that the feature is extended to longer wavelengths than the $90 \mu\text{m}$ feature. The longer wavelength edge of the interstellar feature cannot be well determined. Although the exact peak position and width of the feature depend on the assumed continuum and the location of the baseline, the interstellar $100 \mu\text{m}$ feature seems to be shifted to longer wavelengths and have a wider width than the $90 \mu\text{m}$ feature seen in evolved stars. While carbonate grains are a likely candidate for the $90 \mu\text{m}$ emission around evolved stars and may partly contribute to the interstellar $100 \mu\text{m}$ feature, we examine the possibility of alternative species which has a broad feature around $100 \mu\text{m}$ for the band carrier in the diffuse emission. In the following we investigate whether carbon onion grains consisting of concentric curved graphitic sheets (Ugarte 1992) can account for the observed broad $100 \mu\text{m}$ feature or not.

3.3. Far-Infrared spectrum of carbon onion particles

Graphite is an anisotropic material and has different optical properties in the directions parallel and perpendicular to the c-axis (the c-axis is perpendicular to the graphitic plane). It has an interband transition around $80\mu\text{m}$ in the direction perpendicular to the c-axis (Philipp 1977). The emission efficiency of graphite spheres can be calculated by the so-called $\frac{1}{3}-\frac{2}{3}$ approximation (Draine & Malhotra 1993), in which the efficiencies in the perpendicular and parallel to the c-axis are averaged with the weight of $\frac{2}{3}$ and $\frac{1}{3}$, respectively. This approximation is valid in the small particle limit if the sphere consists of layered graphitic sheets and the optical properties in both directions are independent. In the graphite sphere, the emission efficiency in the direction parallel to the c-axis is much larger than that in the direction perpendicular to the axis in the far-infrared region. Therefore the interband transition feature mentioned above is not visible in the averaged efficiency (Draine & Lee 1984).

In carbon onions, on the other hand, the graphitic layer is curved and approximately constitutes closed shells. Thus the optical properties in the both directions should be mutually coupled and the interband feature can become visible in the emission efficiency of carbon onion grains. Figure 5 shows the emission efficiency factors divided by the grain radius for a graphite sphere and a carbon onion grain under the assumption that the grain radius is much smaller than the wavelengths in question. Here the dielectric constants of graphite in the directions parallel and perpendicular to the c-axis at room temperature measurements are adopted in the calculations (Philipp 1977; Venghaus 1977, see below for discussion). The efficiency for the carbon onion is calculated by the formulation by Henrard et al. (1993) and is assumed to have a central cavity of 0.7 in radius relative to the particle size. The appearance of the feature is insensitive to the size of the cavity. A broad feature around $100\mu\text{m}$ is seen in the emission efficiency of the graphite sphere in the direction perpendicular to the c-axis, but it is hardly seen in the averaged efficiency. On the other hand, the far-infrared feature is evident in the emission efficiency of carbon onion particles.

Figure 6 shows a comparison of the observed feature with that of carbon onion grains. To make the comparison easy the observed spectra are divided by the assumed continuum, while the efficiency of the carbon onion is divided by $\lambda^{-2.2}$. Two lines in the upper two panels indicate the effect of the assumed continuum. Carbon onion grains show a similar broad feature to that observed in the diffuse interstellar emission, but details of the profile do not match perfectly. Taking account of the uncertainties in the shape of the underlying continuum and the optical properties of carbon onions (see below), the similarity of the band feature suggests that carbon onions are a possible carrier of the interstellar $100\mu\text{m}$ feature.

The $100\mu\text{m}$ feature of carbon onions results from the surface resonance of small par-

ticles (Bohren & Huffman 1982) and appears near the wavelength where the real part of the dielectric constants in the perpendicular direction just becomes below zero. The exact position and profile of the feature thus depend on the adopted dielectric constants. While the electronic structure of carbon onions has been suggested to not differ significantly from that of graphite (Pichler et al. 2001), the contribution of free electrons, which dominates in the far-infrared regions, may be different. In fact, measurements of electron spin resonance and electron energy-loss spectroscopy suggest that π electrons in carbon onions are mostly localized in small domains (Tomita et al. 2001). The localization of π electron will decrease the contribution of free electrons, shifting the surface mode to wavelengths longer than $100\,\mu\text{m}$. We surmise that the shift can be more than $10\,\mu\text{m}$. But it is difficult to estimate the possible range of the shift because the behavior of free electrons depends also on the temperature and the strength of the interband transition in carbon onions could also be affected by the localization. The π electron localization, the temperature dependence, and the possible change in the interband transition strength should affect the optical properties of carbon onions in the far-infrared. The match seen in Figure 6 may be just a coincidence in this sense. The present calculation suggests that the observed band feature can be accounted for if carbon onion grains contribute to 20–30% of the far-infrared emission.

Carbon is an abundant element, but the exact form of carbon dust in the interstellar medium is not yet clear (e.g. Nuth 1985). Carbon onions are a likely form other than graphite or amorphous carbon in addition to small aromatic particles or large molecules whose presence has been confirmed by the infrared emission bands in the diffuse interstellar radiation (Onaka et al. 1996; Mattila et al. 1996). Carbon onions have recently attracted attentions as a new form of carbon material following the discovery of fullerenes and their family. In astronomy, they are suggested to be formed in interstellar processes (Ugarte 1995) and the harsh conditions accompanying interstellar dust formation are favorable for the formation of onions (Henrard, Lambin, & Lucas 1997). They have been proposed as a likely candidate for the interstellar 220 nm extinction hump (Henrard, Lucas, & Lambin 1993). The quenched carbonaceous composite (QCC), which shows a feature similar to the interstellar 220 nm hump (Sakata et al. 1983), has also been shown to contain graphitic shell structures (Wada et al. 1999). It is not unexpected that the band features of carbon onions, if exist, also appear in the infrared region. In the present paper we simply propose the possibility that the interband feature of graphite in the far-infrared could appear in the emissivity spectrum of particles consisting of curved graphitic sheets and the observed broad interstellar feature around $100\,\mu\text{m}$ may be accounted for by carbon onion grains. Experimental work is definitely needed for further investigations.

4. Summary

In the present paper we reported the detection of two far-infrared features at $65\,\mu\text{m}$ and $100\,\mu\text{m}$ in the diffuse infrared emission. The $65\,\mu\text{m}$ band can reasonably be attributed to the Ca-rich silicate, diopside. If this identification is correct, this is the first detection of a crystalline silicate feature in the interstellar diffuse emission. The interstellar $100\,\mu\text{m}$ feature seems to be broader and peaked at longer wavelengths than the calcite feature seen in evolved stars although the precise estimate of the band profile is difficult. As a possible band carrier we investigate the possibility that the feature originates from carbon onion grains. While the observed feature may be accounted for by carbon onion grains if the assumed optical properties are adequate, the appearance of the feature is sensitive to the electronic structure of carbon onions. The origin of the interstellar $100\,\mu\text{m}$ feature must be investigated in further experimental studies.

The authors thank K. Kawara, Y. Satoh, T. Tanabé, H. Okuda, T. Tsuji, H. Shibai, and other members of the Japanese ISO group for their continuous help and support. We also thank S. Tomita and S. Hayashi for stimulating discussions on the optical properties of carbon onions and H. Chihara and C. Koike for providing us the far-infrared data of diopside and calcite. This work was supported in part by Grant-in-Aids for Scientific Research from the Japan Society of Promotion of Science (JSPS).

REFERENCES

Bohren, C. F., & Huffman, D. R.
1982, *Absorption and Scattering of Light by Small Particles* (New York: Wiley)

Chan, K.-W., & Onaka, T. 2000, *ApJ*, 533, L33

Chihara, H., Koike, C., & Tsuchiyama, A. 2001, *PASJ*, 53, 243

Clegg, P., et al. 1996, *A&A*, 315, L38

Cohen, M., Barlow, M. J., Sylvester, R. J., Liu, X.-W., Cox, P., Lim, T., Schmitt, B., & Speck, A. K. 1999, *ApJ*, 513, L135

de Graauw, T., et al. 1996, *A&A*, 315, L49

Demyk, K., Jones, A. P., Dartois, E., Cox, P., & d'Hendecourt, L. 1999, *A&A*, 349, 267

Draine, B. T., & Lee, H.-M. 1984 *ApJ*, 285, 89

Draine, B. T., & Malhotra, S. 1993, *ApJ*, 414, 632

Feinstein, A. 1995, *Rev. Mex. Astron. Astrofis.*, 2, 57

Gry, C., et al. 2002, ISO Handbook; Volume IV: LWS—The Long-Wavelength Spectrometer, version 2.0 (ESA)

Henrard, L., Lucas, A. A., & Lambin, Ph. 1993, *ApJ*, 406, 92

Henrard, L., Lambin, Ph., & Lucas, A. A. 1997, *ApJ*, 487, 719

Hildebrand, R. H. 1983, *QJRAS*, 24, 267

Jones, A. P., Tielens, A. G. G. M., & Hollenbach, D. J. 1996, *ApJ*, 469, 740

Kemper, F., Jäger, C., Waters, L. B. F. M., Henning, Th., Molster, F. J., Barlow, M. J., Lim, T., & de Koter, A. 2002, *Nature*, 415, 295

Kessler, M. F., et al. 1996, *A&A*, 315, L27

Koike, C., et al. 2000, *A&A*, 363, 1115

Mattila, K., Lemke, D., Haikala, L. K., Laureijs, R. J., Leger, A., Lehtinen, K., Leinert, C., & Mezger, P. G. 1996, *A&A*, 315, L353

Mizutani, M., Onaka, T., & Shibai, H. 2002, *A&A*, 382, 610

Molinari, S., Ceccarelli, C., White, G. J., Saraceno, P., Nisini, B., Giannini, T., & Caux, E. 1999, *ApJ*, 521, L71

Molster, F. J., Lim, T. L., Sylvester, R. J., Waters, L. B. F. M., Barlow, M. J., Beintema, D. A., Cohen, M., Cox, P., & Schmitt, B. 2001, *A&A*, 372, 165

Molster, F. J., Waters, L. B. F. M., & Tielens, A. G. G. M. 2002, *A&A*, 382, 222

Murakami, H., et al. 1996, *PASJ*, 48, L41

Nuth, J. 1985, *Nature*, 318, 166

Okada, Y., Onaka, T., Shibai, H. & Doi, Y. 2002, *A&A*, submitted

Onaka, T., Yamamura, I., Tanabé, T., Roellig, T. L., & Yuen, L. 1996, *PASJ*, 48, L59

Philipp, H. R. 1977, *Phys. Rev. B*, 16, 2896

Pichler, T., Knupfer, M., Golden, M. S., Fink, J., & Cabioc'h, T. 2001, Phys. Rev. B, 63, 155415

Sakata, A., Wada, S., Okutsu, Y., Shintani, H., & Nakada, Y. 1983, Nature, 301, 493

Savage, B. D., & Sembach, K. R. 1996, ARA&A, 34, 279

Smith, R. G., Robinson, G., Hyland, A. R., & Carpenter, G. L. 1994, MNRAS, 271, 481

Tomita, S., Sakurai, M., Ohta, H., & Hayashi, S. 2001, J. Chem. Phys., 114, 7477

Ugarte, D. 1992, Nature, 359, 707

Ugarte, D. 1995, ApJ, 443, L85

Venghaus, H. 1977, Phys. Stat. Solidi (b), 81, 221

Wada, S., Kaito, C., Kitamura, S., Ono, H., & Tokunaga, T. A. 1999, A&A, 345, 259

Waelkens, C., et al. 1996, A&A, 315, L245

Walborn, N. R. 1995, Rev. Mex. Astron. Astrofis., 2, 51

Waters, L. B. F. M., et al. 1996, A&A, 315, L361

Yang, J., & Fukui, Y. 1992, ApJ, 386, 618

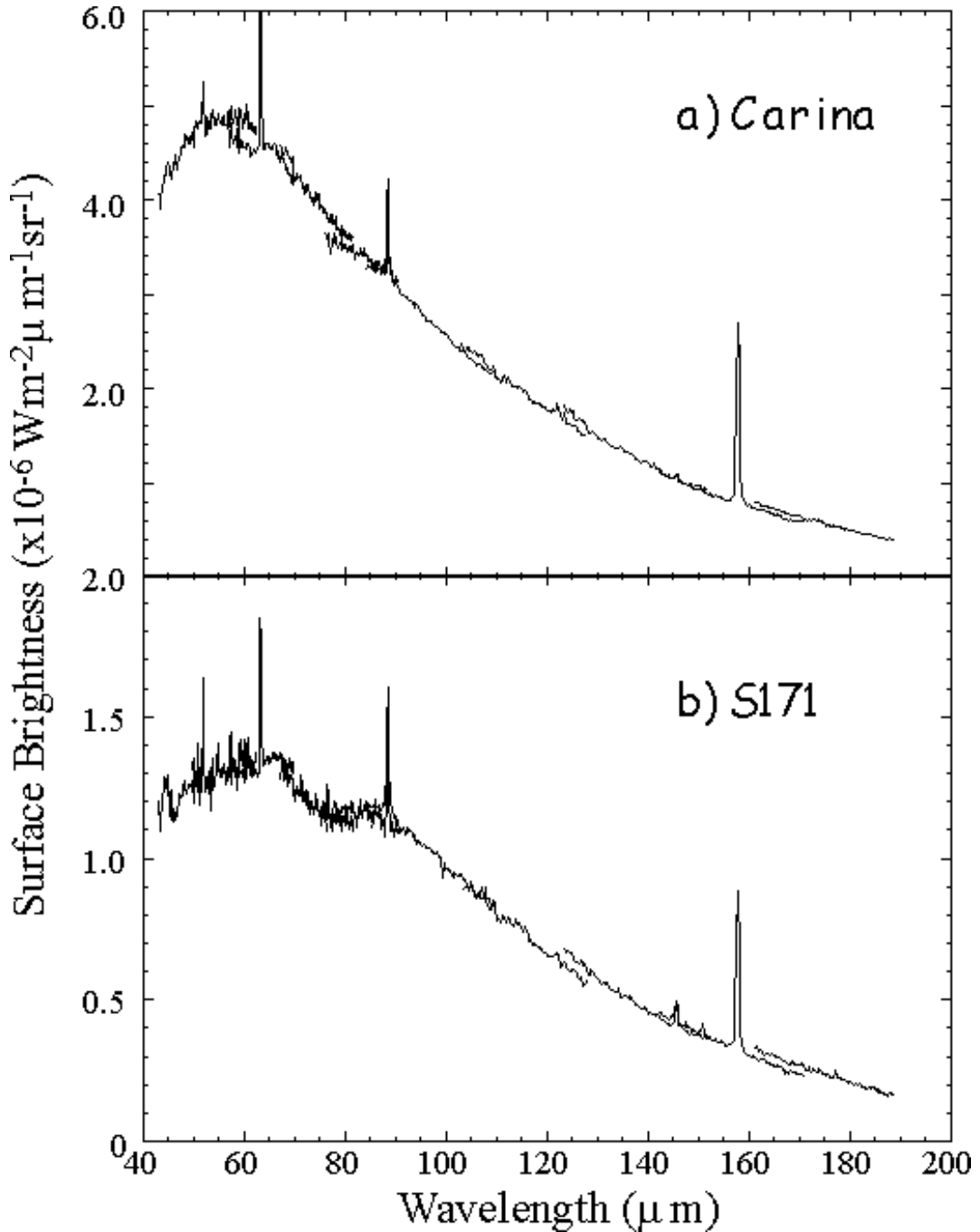


Fig. 1.— Examples of unstitched LWS spectra of the Carina nebula (a) and the Sharpless 171 (S171) (b). The Carina nebula spectrum was taken at $(l, b) = (287.31^\circ, -0.69^\circ)$, while the S171 spectrum at $(l, b) = (117.95^\circ, 4.98^\circ)$. Strong sharp lines are [O I]63 μm , [O III]88 μm , and [C II]158 μm .

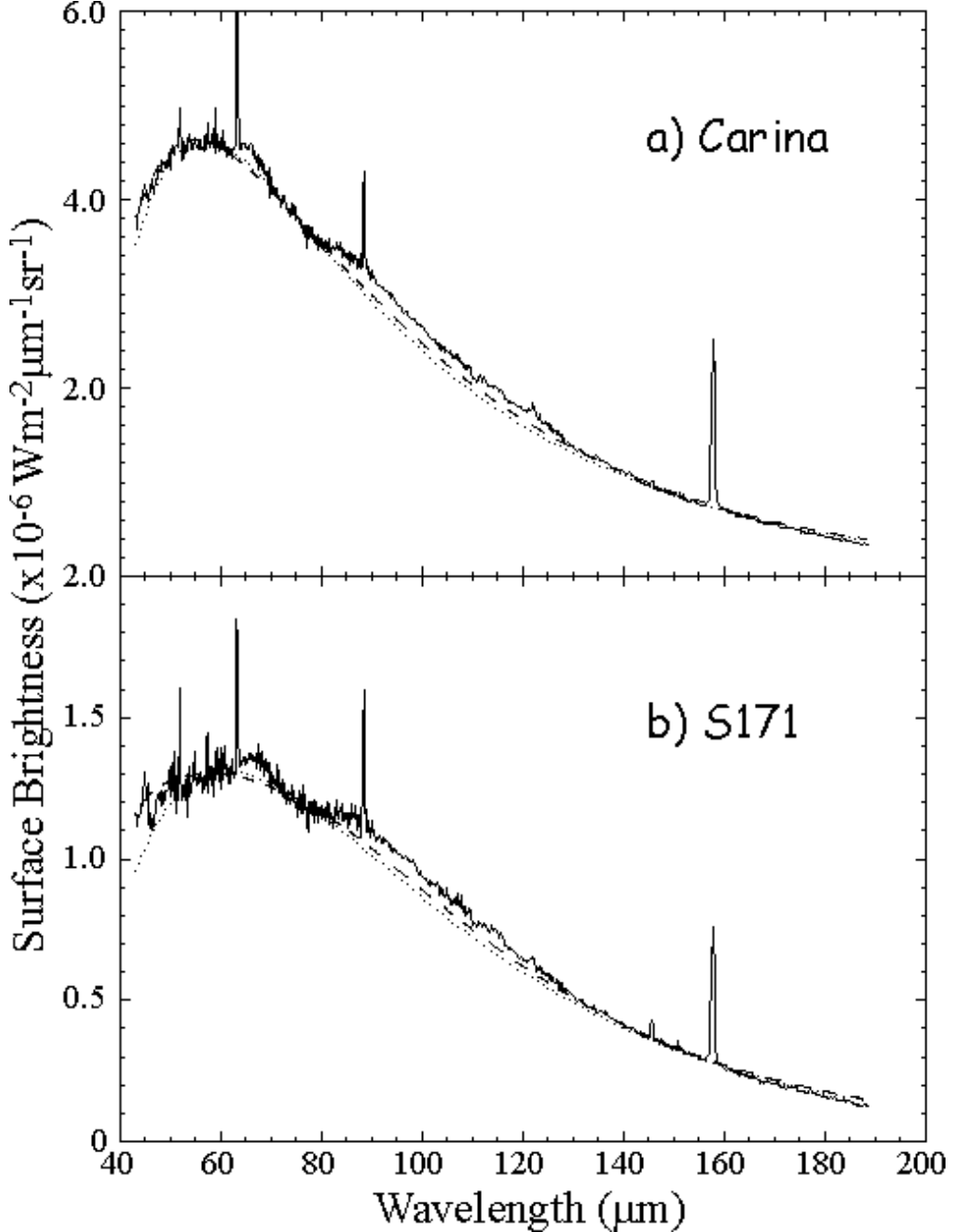


Fig. 2.— Stitched spectra of the Carina nebula (a) and the Sharpless 171 (b) of Figure 1. The best fit continua of the astronomical silicate and graphite model are also indicated. The dotted lines indicate the fitted continuum to 140–190 μm (case A), while the dashed lines indicate that to 120–190 μm (case B; see text). The temperatures of silicate and graphite grains are, 21.7K and 39.2K, 23.3K and 41.1K for the Carina and S171 regions for case A, respectively. They are 23.0K, 42.0K for the Carina region, and 24.4K and 49.9K for the S171 region for case B.

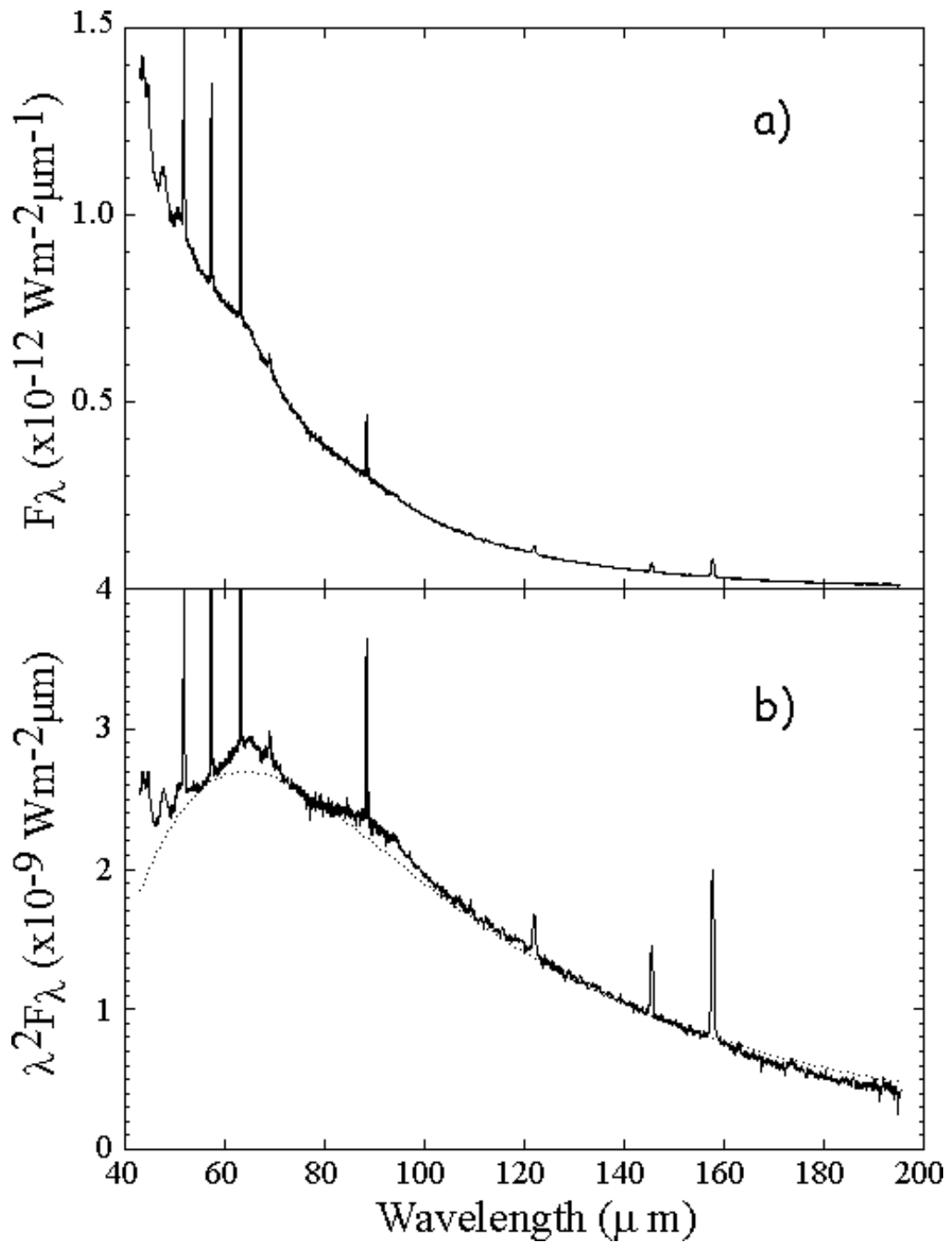


Fig. 3.— Spectrum of NGC6302. The dotted line indicates a graybody of 51.8K with $\beta = 1.4$ (see text).

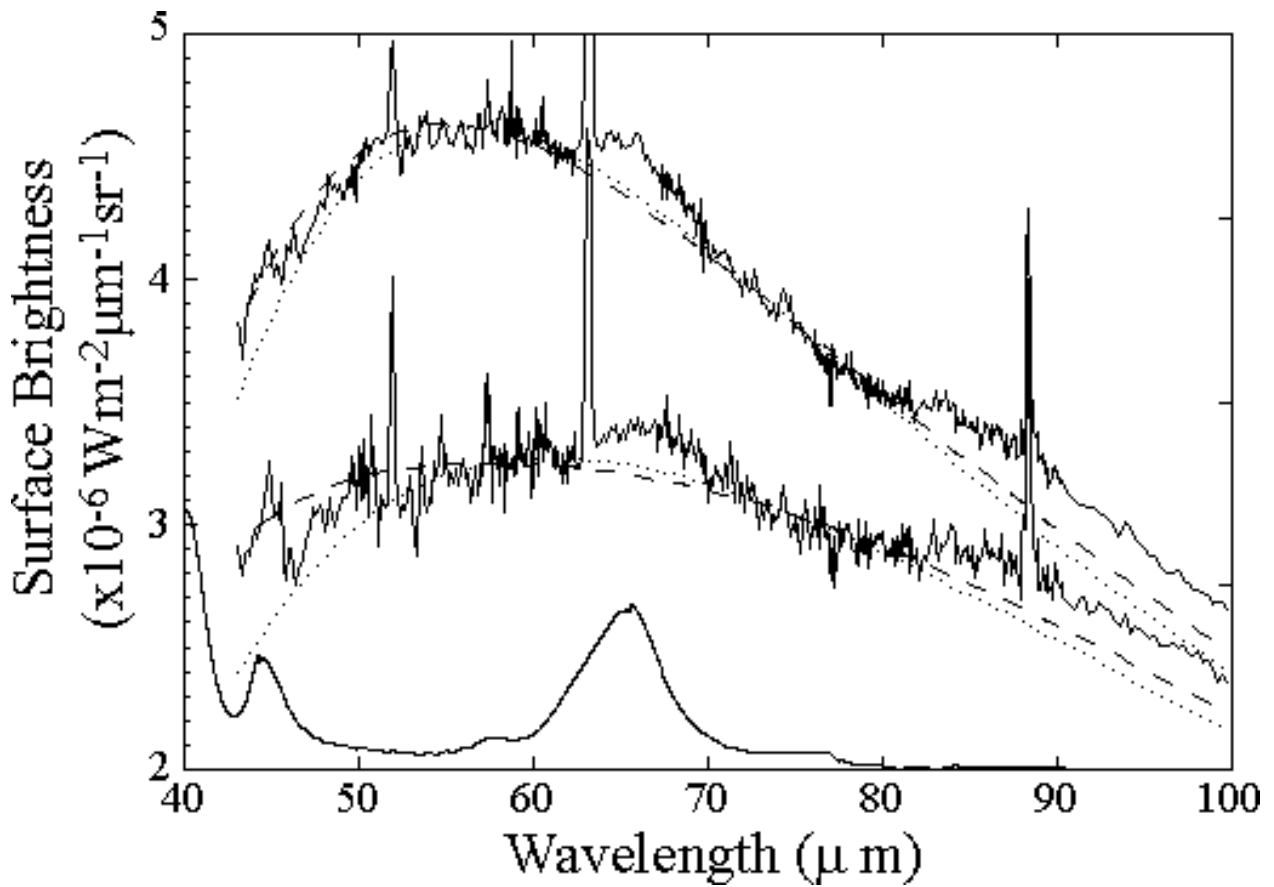


Fig. 4.— The spectra of 40–100 μm of the Carina (upper curve) and S171 (middle curve) and the absorption coefficient of diopside at 4 K (lower curve; Chihara et al. 2001). The spectrum of S171 is multiplied by 2.5. The same best fit continua are also plotted as in Figure 2.

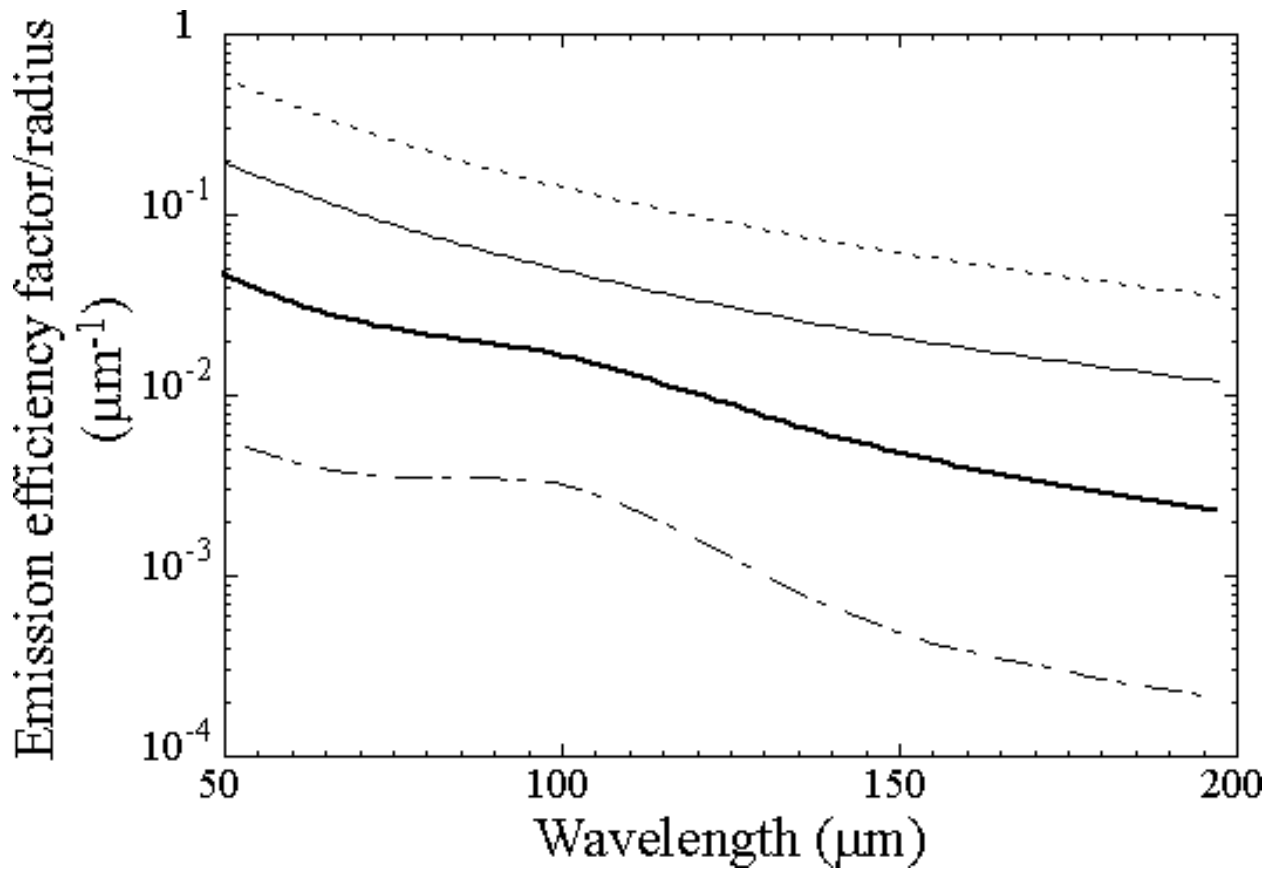


Fig. 5.— The emission efficiency factors divided by the particle radius for carbon onions (thick solid line) and graphite grains (thin solid lines). Those for graphite grains in the direction perpendicular to the c-axis (dot-dashed line) and those parallel to the c-axis (dashed line) are also plotted. Carbon onion grains are assumed to have a cavity of 0.7 in radius relative to the particle radius.

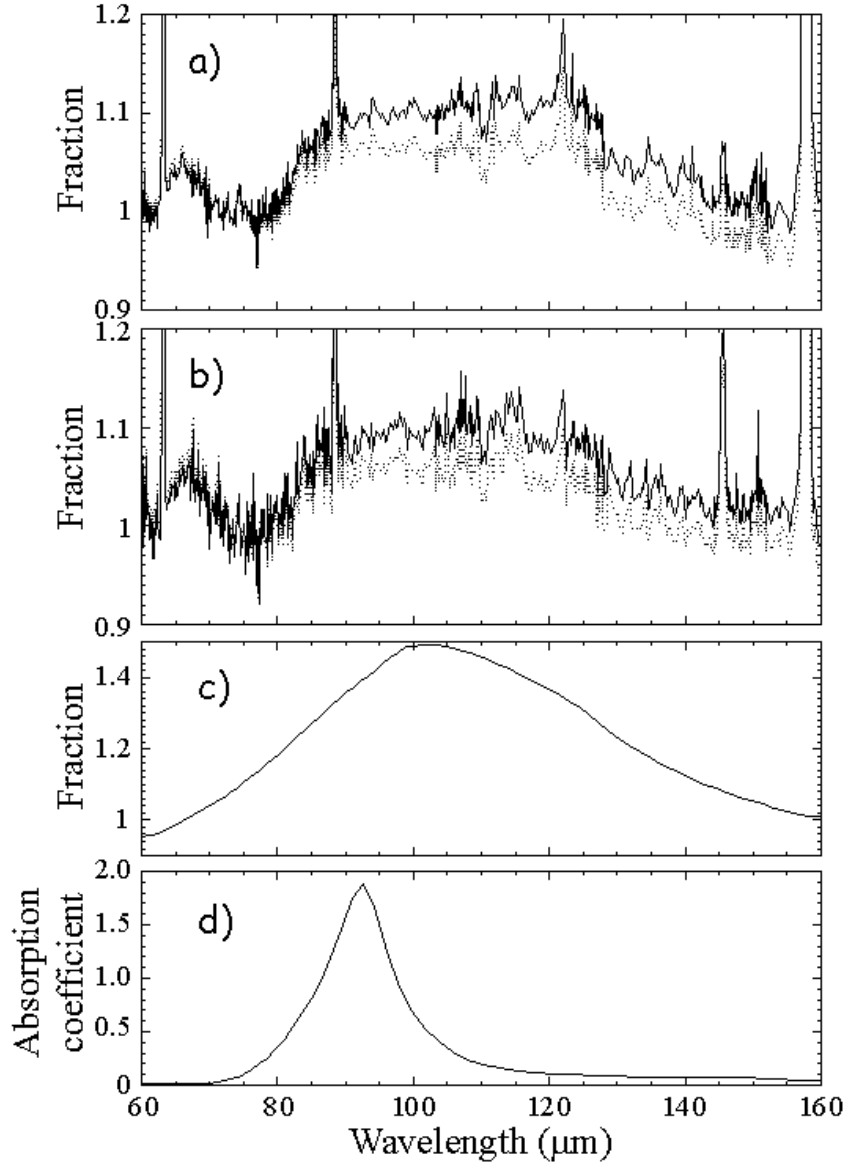


Fig. 6.— Comparison of the carbon onion feature (c) with the observed interstellar feature in the Carina nebula (a) and S171 (b) together with the absorption coefficient of calcite (d; C. Koike, 2002, private communication). The fractions of the spectra to the assumed continuum are plotted for (a), (b), and (c). In (a) and (b) two lines indicate the effects of the assumed continuum. The solid line shows the result of case A (140–190 μm baseline), while the dotted line indicates that of case B (120–190 μm baseline) (see text).